INDUCTION MOTOR FAULT DETECTION AND CLASSIFICATION USING RCNN AND SURF BASED MACHINE LEARNING ALGORITHMS AND INFRARED THERMOGRAPHY

B.Sasikumar*, Associate Professor, Department of Artificial Intelligence and Data Science, Knowledge Institute of Technology, Salem, Tamil Nadu, India, Tel.: +91-9894824645, Email: balusasiskg@gmail.com

Dr.K.Venkatasalam, Associate Professor, Department of Computer Science and Engineering, Mahendra Engineering College, Namakkal, Tamil Nadu, India, Tel.: +91-9952815592, Email: venkispkm@gmail.com

Dr.P.Rajendran, Professor, Department of Computer Science and Engineering, Knowledge Institute of Technology, Salem, Tamil Nadu, India, Tel.: +91-9443264741, Email: peerajendran@gmail.com

Abstract

Induction motors in electrical industries face stress and potential faults. Preventive maintenance, including fault detection, is vital for safety and energy conservation. Infrared imaging, though underutilized, can monitor machine conditions effectively. In response to this gap, this paper presents a novel motor fault identification method employing infrared thermography (IRT) in combination with image processing and machine learning techniques, with a particular focus on energy efficiency. IRT is harnessed for early fault detection to promote energy conservation. The approach involves the extraction of color and texture features from the motor's infrared images using the Gabor filter and GNS (Global Neighbourhood Structure) map. The proposed method integrates the faster R-CNN (Region-based Convolutional Neural Network) with the SURF (Speeded Up Robust Features) algorithm to enhance fault detection and classification accuracy. SURF serves as a feature descriptor for faster R-CNN, enabling object detection and fault classification based on the extracted features. Additionally, efficiency is assessed using the Finite Element Method (FEM) based on stator and rotor power, contributing to energy conservation through early fault detection in motors. Notably, the proposed motor fault classification is applicable under various loading conditions, consistently achieving accuracy rates exceeding 90%.

Keywords: Motor Fault Identification, Machine learning methods, Infrared thermography, integrated faster RCNN-SURF classifier, Finite Element method

1. Introduction

Induction motors can be mostly used in industrial, commercial and housing applications as they give significant merits over other kinds of electric motors. Compared to other rotating machines, the induction motors contains some good features such as robust, inexpensive, less maintenance, etc. However, faults have risen in induction motor during various construction or operating stresses. In induction motors, bearing faults, stator faults, and rotor bars faults can occur recurrently. Depending on the survey report, the induction motors' component percentage can be bearing (41%), rotor faults (10%), winding (37%), and others (12%). These failures will direct to high energy consumption or poor efficiency, high production loss and fatal accidents can also be happened in some cases. Therefore, early detection of induction motor faults is most significant to the economical operation and energy conservation. Now a day, motor fault detection is executed using motor monitoring, initial fault recognition, and fault diagnosis. In the production line, the condition monitoring and induction motor's fault diagnosis is performed as the most important process and it is operated as an efficient tool to decrease downtime and production losses.

The most condition monitoring methods were used to induction motor fault diagnosis depending on vibration and current. These vibration and current based methods have been applied effectively for various electrical and mechanical related faults detection. Agoston [1] has presented few electrical and mechanical failures in induction motors according to the motor vibration based condition monitoring. The definite frequencies have been detected using monitoring and analysing of the vibration spectrum for the fault detection. De Araujo Cruz et.al [2] have presented a hybrid method that has utilized the data obtained from vibration and current sensors for fault detection at an early stage. However, both these vibration and current based condition monitoring techniques use costly sensor devices, data acquisition methods and a lot of time is consumed for fault diagnosis computation. Chang et.al [3] have enhanced a condition monitoring method that contains fault diagnosis analysis (FDA) and operating condition monitoring (OCM). The vibration detection approach has been utilized by the OCM depending on the ISO 10816-1 and NEMA MG-1 international standards, and the vibration-electrical hybrid method was employed by the FDA according to the different indices. In this study, the voltage and current sensors were utilized because of their high safety and expediency. Conversely, it is

needed in additional setup or relays to identify the winding fault so, its purpose has been limited only to high stress or vital motors due to it most expensive.

Existing bearing faults, rotor faults detection methods were used depending on the spectrum examination of motor voltage, motor current, and instant input power. Contreras-Hernandez et.al [4] proposed a motor fault recognition method using quaternion signal analysis. In this study, the quaternion coefficients were determined as the motor current capacity values, and the variables x, y, and z have been used as the measurements from a triaxial accelerometer accumulated on the induction motor framework. But, this method will be hard to attain the precise models of faulty motors and also to apply model-based methods. Chen et.al [5] used an artificial neural network (ANN) for the fault detection of high-voltage motors. The relationship between stator failures and pattern features were established depending on the partial discharge (PD) information estimation. However, PD tests can be an offline test, in which a motor shutdown is required that will direct to loss of production. Thus, noncontact and online monitoring is needed for fault detection.

Infrared thermography (IRT) can be utilized as an online and non-contact type condition monitoring method and it is mostly utilized to inspect transformers and electrical installations. It is operated as a device, in which the infrared energy is captured that can be transmitted from an object to its environment and a real-time image will be produced in a color palette [6]. For the motor fault diagnosis, this kind of tool is used since the prospect to point out the operating condition of the object using its temperature range. Javed et.al [7] applied Machine Vision (MV) that has utilized IRT for the inter-turn fault detection in induction motor drive using support vector machine (SVM). Mahami et.al [8] proposed an infrared-based method to identify three phase's induction motor faults. For the fault feature extraction, bag-of-visual-word (BoVW) method was utilized with SURF method. This method was done using isothermal representations, in which the temperature gradient has been visualized and, therefore, the localization of the failure source was facilitated. Nevertheless, IRT is left underutilized for motor's health monitoring and fault diagnosis of motors. According to the thermal model, temperature evaluation can be flexible and precise; however, it will not respond to the alterations in motor thermal distinctiveness. In induction motors, the efficiency of thermographic methods for fault recognition will be very reliant on its accurateness during the hot areas identification

and its severity level prediction. Therefore, in this paper, efficient image processing and machine learning methods are used with IRT devices to overcome the above issues.

Several motor fault detection methods are done depending on the current and vibration spectral analysis by applying Fourier transform and wavelet transform [9-11]. In this study, 3D-DWT is applied for effective image decomposition. Ge et.al [12] utilized a fault discovering scheme according to an empirical wavelet transform sub-model hypothesis examination and uncertainty correlation categorization to analyse the rolling bearing failures by applying the vibration signals. Conversely, the authors determined only on rolling bearing failures. Many existing methods have used the ANN and SVM (Support Vector Machine) classifier for the induction motor fault classification [13-15]. Agrawal and Jayaswal [16] proposed a comparative analysis between SVM and ANN by applying the energy entropy models and the continuous wavelet transforms to detect and classify the rolling component bearings. However, accurate motor fault classification is not provided by these classifiers because ANN has to discover the most suitable training group and SVM can only use two classes for fault classification. Jayaswal and Wadhwani [17] have given a survey on ANN, and wavelet transform, and fuzzy logic that has been utilized to identify rotating machinery failures employing raw vibration signals. But, this work has given special attention trolling component bearing faults.

Machine learning and deep learning methods are used in advanced compared to customary image processing methods. The machine learning methods have been utilized widely in machine health due to its probable methods of featuring demonstration. Ali et.al [18] have presented a practical machine learning-based fault detection system for induction motors. The authors have utilized the three classification methods such as SVM, K-Nearest Neighbours (KNN), and ensemble, with seventeen various classifiers given in MATLAB Classification Learner toolbox. Xu et.al [19] have used a technique according to the deep CNN and random forest ensemble learning with a significant presentation; though, the authors only focused on bearing fault detection. Lu et.al [20] have applied a probabilistic neural network (PNN) as an image classifier using the conversion of signals to images by applying a bi spectrum monitoring methods. Though neural networks methods using raw data signals have been used in numerous research works for the fault detection and categorization, the data preprocessing can be a very significant task in deep learning or machine learning methods [21]. Several research works have

utilized time-frequency, frequency, and histograms for the conversion of signals into images to classify images [22-24]. Rahmat et.al [25] have presented that the faster R-CNN is not provided more accuracy for image classification and it takes more time to execute. Therefore, the faster RCNN is integrated with SURF to enhance motor fault classification accuracy. The benefit of using R-CNN over a neural network is its ability to develop an internal representation of a two-dimensional image or a matrix of values. It helps the model to learn the position and scale of different structures in the image data or the two-dimensional matrix data. It also helps to reduce the number of parameters involved by learning high-level features and via the reusability of weights. Khamisan et.al [26] used a SURF method for induction motor thermal image segmentation. The SURF algorithm is used as a good feature descriptor for the image classification. Therefore, in this paper, the advantages of RCNN and SURF are used to enhance classification accuracy for the induction motor fault detection. Many research works have focused only on bearing faults. But, in this paper, the stator, rotor, and bearing faults are detected using improved machine learning methods.

For the vibration analysis, specialized equipment is needed like accelerometers and data acquisition systems that could be expensive to purchase and maintain. Vibrating machinery makes high frequency noise, cause safety problems and direct to ruin in plant operating situations. For the current analysis in condition monitoring, it is needed to install MCSA (Motor Current Signature Analysis Sensors), conversely, MCSA technique's presentation was ruined through the augmentation of the load directly changing the fault indicator's amplitude. Besides, and as reported by numerous examinations, the frequencies connected with this kind of fault depend on the exact motor status. Thus, in this paper, thermography-based method is applied since it contains the following advantages non-contact detection, freedom from electromagnetic interference, safety, reliability and providing large inspection coverage compared to vibration and current based fault detection method.

2. Proposed Methodology

In this paper, thermal imaging is used as a diagnostic tool for the induction motor's health and energy monitoring by observing the cause of failure. During an operation, IRT is used for

monitoring, motor's abnormal condition identification. By using this tool, an early warning can be given to the operator or technician through the rotating machine's temperature signatures. In the proposed method, the SURF is integrated with faster R-CNN to improve the image classification for motor fault detection. The proposed system architecture has been illustrated in figure 1. From figure 1, IRT training data is taken for the motor's energy monitoring and fault detection. Initially, image preprocessing is computed by applying the 3D-DWT (3D- Discrete Wavelet Transform). Afterward, the Gabor filter and the GNS map are used to extract the color and texture features from the decomposed thermal image of induction motor according to the bearing, stator and rotor characteristics or temperature variations. Subsequently, the proposed integrated classifier model is trained with selected features. Based on the selected features, the classifier classifies the induction motor into fault motor (bearing faults, stator faults, rotor faults, or healthy motor). The motor efficiency is estimated by applying the finite element method for energy monitoring. Hence, the energy can be conserved by early detection of a motor fault.

The following phases are used by the proposed method to detect induction motor fault at an early stage for the energy conservation:

- Image acquisition
- Image pre-processing using 3D-DWT
- Feature Extraction using Gabor and GNS map
- Image classification using integrated faster RCNN-SURF
- Efficiency estimation using FEM

2.1. Experimental Test Bench For image acquisition

Experimental test bench is an environment utilized to testing the proposed method with the help of software and hardware tools. Figure 2 shows the experimental test bench to compute the proposed method. A 0.5 hp, 440 V, 4 poles, the star-connected three-phase induction motor can be used for testing the fault conditions treated in this work. Induction motor's thermal images will be captured by using the thermal camera FLIR A615 under different load conditions such as full load, half-load and no-load. By using this infrared camera, motor images are captured at every second and the infrared camera is fitted with a fire-wire connection. A thermal camera is also connected with a portable computer and it can be given with an acquisition and

analysis tool Tensorflow. The captured images' data is stored in the computer and then images can be examined using Tensorflow tool. This tool will permit the captured images' visualization and allows precise temperature estimation and its exportation for pre and post-processing using effective data mining and machine learning methods. Besides, other measuring devices are also connected such as power analyser, digital tachometer, and torque transducer to constantly observe speed, electric power, and the mechanical torque to calculate the motor's efficiency. The sample thermal images of induction motor have been illustrated in figure 3. In this work, thermal images are acquired using the following conditions: Healthy, Rotor Bar Fault, Abnormal Stator, Normal Bearing, Abnormal Bearing, Inner race defect, Outer race defect, and lubrication lack.

2.2. Image Pre-processing using 3D-DWT

Initially, the third decomposition level of the 3D-DWT is applied to the induction motor's thermal images for the process of image preprocessing. The DWT method has given efficient performance and better ranks all among the decomposition methods. In both frequency and time domain, the multi-resolution examination can be executed by this method. Therefore, this paper applies the 3D-DWT to attain better image decomposition for further processes such as feature extraction and selection, and fault classification. In the 3D-DWT, the thermal image data is separated into frequency sub bands and it can give advanced image decomposition than the 2D-DWT method. 3D data cubes correlation has been measured in this process that can be used to enhance the compression. The fundamental design will be to provide a signal as a wavelet superposition. 3D-DWT is computed on thermal images using one-dimensional DWT filter banks on three spatio-spectral dimensions. The wavelet decomposition is applied on target image to three spatial directions (a,b,c) and then three-dimensional wavelet components are attained. The 3D-DWT is constructed by a tensor product:

$$(TI)^{(a,b,c)} = \left(L^a \oplus H^a\right) \otimes \left(L^b \oplus H^b\right) \otimes \left(L^c \oplus H^c\right) \quad (1)$$

In equation (1), $\oplus$denotes the direct sum and $\otimes$ represents the tensor product. a,b,c represents directions in the horizontal and vertical domains, and the spectral dimension of the

thermal image. L denotes the low pass filter and H can be the low and high-pass filters along three dimensions.

Two-level of 3D-DWT has been established in figure 4. In this process, low pass and high pass filters can be employed to a-dimension to filter the $f(a,b,c)$ volume to get sub-bands L and H. Subsequently, filters are utilized along to b -dimension and hence LL, LH, HL, and HH images will have happened. 3D-DWT can filter the c-dimension of these four sub-bands. As a result, the eight sub-bands of the target thermal image will be attained such as LLL, LLH, LHL, LHH, HLL, HLH, HHL and HHH.

2.3. Feature Extraction using Gabor and GNS map

After the image decomposition, a technique is used to extract color features such as skew, entropy, mean, standard deviation, and kurtosis from thermal images using Gabor filters-GNP map to the data for classification work. In this method, the RGB image is transformed to L* a* b* color space, therefore, it contains three values such as L, a and b. The values of L can represent the grayscale color space from these values for the texture feature extraction whereas the color feature is represented by the a and b values.

The macro-texture is extracted by Gabor filters using the following equation (2):

$$G_{\lambda\varphi\sigma\gamma}(a,b) = e^{-\frac{\hat{a}^2+\gamma^2+\hat{b}^2}{2\sigma^2}} \cos\left(2\pi\frac{\hat{a}}{\lambda}+\varphi\right) \qquad (2)$$

Where,

$\hat{a} = a\cos\theta + b\sin\theta$

$\hat{b} = -a\sin\theta + b\cos\theta$

In the equation, λ denotes the sinusoidal factor's wavelength parameters. λ will be acted as the wave's inverse of the frequency in the Gabor function with a value of $f = \frac{1}{\lambda}$. θ can be the standard direction of the Gabor function's equivalent lines and its value is established between 0^o and 360^o. The phase offset is represented by φ as a factor in the cosine Gabor function and its value in the range betwee$0^o$and 180^o. σ Indicates the Gaussian factor's standard

deviation that establishes the support size of the Gabor function and the value of σ will not be firmed straight however it may be altered only using the bandwidth value (b). γ can be the spatial aspect ratio, in which Gabor function's eclipse shape is determined. Shape is in the form of circle if $\gamma = 1$. Elongated shape is formed in the orientation function when $\gamma < 1$.

The micro-texture will be extracted by applying the GNS map. In this kind of feature extraction method, the intensity similarities are measured between the pixels present in the thermal image. The given pixel x 's intensity similarities to its surrounding pixels within a definite local region or search window Ws is used and it is estimated through the Euclidean distance and it is given by:

$$d^2(x,y) = \| v(N_x) - v(N_y) \|^2 \tag{3}$$

where pixel x is positioned at the $m \times m$ search window's centre point and $v(N_x)$ represents the neighbourhood pixel values vector around x that has been surrounded by the $n \times n$ adjacent window W_n. Besides, y denotes the search window's all pixels and $v(N_y)$ can be operated as the adjacent pixels vector within the adjacent window. The Euclidean distance between neighbourhood pixels N_x and N_y can be represented by $\|.\|$ and it has been more effectual to produce generated texture features to be extremely robust to arbitrary noise compared to Euclidean distance estimation in individual pixel values. After that, the local neighbourhood structure map will be produced using every Euclidean distance replacement with the search window's every pixel value.

For extracting features from the thermal image, a GNS map is computed and the local neighbourhood structures average is measured for the chosen pixels. Each entry q can be located in the GNS map and it is given by:

$$GNS(q) = \frac{1}{n} \sum_{p \in X} d^2(p,q) \tag{4}$$

In equation (4), X can be the set of chosen thermal image pixels, $d^2(p,q)$ represents any entry in the region structure map produced for pixel p in X, and n denotes the number of GNS maps in the set X that perform normalization.

2.4. Image classification using integrated faster RCNN-SURF

In this proposed method, the SURF and faster R-CNN methods are combined after the feature extraction to acquire accurate induction motor fault detection and classification in thermal images. The enhanced classification algorithm uses only the advantages of SURF and faster R-CNN. The classification process has been illustrated in figure 5. The extracted features are become the input of SURF, in which set of features are selected and described with the predicted scores. In this process, the SURF is used as a feature descriptor of faster R-CNN to detect and classify the faults. Firstly, extracted features between reference and target thermal image are described and pre-matched by the SURF algorithm, then faster R-CNN is to classify the faults into bearing, stator, rotor, or other faults according to the described and matched features by eliminating the false object matching.

The proposed integrated faster RCNN-SURF architecture is given in figure 6. The faster RCNN-SURF classification is done using the following phases:

Input Layer: The extracted features are given as input to the SURF feature descriptor through the CNN.

Proposed Region: In this phase, the features are matched with reference images using the SURF feature descriptor. Afterward, ROI pooling is generated by faster R-CNN to generate a fixed-size feature map from non-uniform selected and matched features that has made by SURF using max-pooling on the inputs. This ROI pooling can be used to speed up the training and test time.

Fully connected Layers: Subsequently, two various fully-connected layers are utilized to produce detection for every one of the objects in the thermal images. It can detect and classify the thermal images in computer vision.

Output Layer: Finally, the classified images are produced in the output layer

Proposed faster RCNN-SURF Algorithm

Input: Extracted features, Feature vector V or Feature point

Output: Classified Images

Step 1: To read the Feature vector V

Step 2: To initialize feature point V with SURF method based on the extracted color and texture features (CO_2 emission, Temperature, Torque, speed, air gap, etc)

Step 3: To fix the feature point in the main position's main direction depending on the chosen length's main direction that has been divided into 4 x 4 sub-regions

Step 4: To compute feature descriptor by SURF algorithm using the following feature vector:

$$V = \left(\sum dx, \sum dy, \sum |dx|, \sum |dy|\right) \quad (5)$$

Where, dx denotes the Haar wavelet response in the horizontal direction, dy represents the Haar wavelet response in the vertical direction.

Step 5: To gather dx and dy response in a horizontal and vertical direction independently in every sub-region and afterward, to gather $|dx|$ and $|dy|$ separately for getting the intensity variation's polarity in the thermal image.

Step 6: To compute the matching process, in which the feature point's SURF descriptor of the target inductor thermal image can be matched with the feature point's SURF descriptor of the reference inductor thermal image.

Step 7: To use matched features as the input of faster R-CNN that establishes a set of regions with the predicted values.

Step 8: To train a faster R-CNN model with extracted and matched features.

Step 9: To re-match the features of the target thermal image with features of reference images by R-CNN with the help of the training and testing process to eliminate mismatched features that have been made by SURF for the fault detection and classification accuracy improvement.

Step 10: To detect and classify Induction motor's Fault into bearing, stator, and rotor faults in the target thermal image according to the accurately matched features

Step 11: Stop

By using this proposed classifier, the motor faults are detected and classified at an early stage. The early detection can be used to reduce the energy consumption in induction motor and also used for energy preservation.

2.5. Efficiency estimation using Finite Element Method

Finally, the efficiency of a healthy induction motor can be estimated by applying the finite element method through the Tensorflow tool. Every finite element simulations can be done in the stator and rotor flux reference frame. In the finite element simulations, both stator and rotor currents will be imposed. A resulting induction machine flux distribution's snapshot for stator current 0.55A and 1280rpm speed has been established in figure 7. In figure 7, rotor and rotor bars, stator and stator bars, shaft, and air-gap are separated using the finite element method to estimate input and output power of induction motor for the efficiency estimation of induction motor.

The efficiency can be defined in the form of the ratio between output to that of input and it is given by:

$$Efficiency\,\eta = \frac{Output}{Input} \tag{6}$$

In this study, 0.5hp three-phase induction motor's rotor and stator efficiency are estimated using the following equations (7) and (8):

$$Rotor\ efficiency = \frac{rotor\ output}{rotor\ input} = \frac{Gross\ mechanical\ \ power\ developed}{rotor\ input} = \frac{P_m}{P_2} \tag{7}$$

$$Stator\ Efficiency = \frac{Stator\ output}{stator\ input} \tag{8}$$

The 0.5hp induction motor efficiency is calculated using the ratio between motor's electrical input to the motor and power developed at shaft and it is given by:

$$Motor\ Efficiency\ \eta = \frac{power\ developed\ at\ shaft}{electrical\ input\ to\ the\ motor} = \frac{P_{out}}{P_{in}} \quad (9)$$

The efficiency between healthy and fault induction motor has been illustrated in figure 8, from the below comparison chart 8, the faulty motor has taken low efficiency compared to the healthy motor because of bearing fault motor can take high voltage output power during the operation; as a result, the energy consumption is increased. Hence, the energy is preserved by using the proposed method through the early detection of motor faults.

3. Results and discussions

. The experimental of the proposed method can be done under the various load conditions such as full load, half-load, and no-load using the Tensorflow tool. In this work, the image preprocessing and the proposed machine learning methods are written in python 3.5 with the Tensorflow as backend and run on the Windows 64-bit operating system shown in table 1. The specifications of the induction motor and the thermal camera have been summarized in table 2. In this experimental result, the attained induction motor's thermal images will be 132 (22*2*3). The sample images of this study are given in figure 9. In figure 9, the experimental thermal images of healthy and faulty induction motor are demonstrated. The image data details are given in table 3 for the feature extraction and classification.

Figure 10 shows the output images of color features representation in the RGB color space to classify motor faults. From chart 10, the color features entropy, mean, skew, and kurtosis are varied based on the standard deviation in the healthy and faulty induction motor. These feature graphs are obtained from the Tensorflow tool, in which, green color represents the rotor fault, red represents the stator fault, black represents the bearing fault, and blue represents the healthy motor. Hence, according to the five-color features, the three-phase induction motor faults are classified. Figure 11 shows the confusion matrix for induction motor fault detection in trail results.

The performance of the proposed method is estimated through no load, half load, and full load conditions, in which i.e. each data set regarded as of 33 thermal images that have been divided into two groups such as training and testing data sets for the fault classification. The acquired thermal images can be compared under the healthy and faulty conditions in the induction motor. Besides, the performance of the proposed method is compared with existing methods ANN, CNN, and SVM [27] in terms of Accuracy, Sensitivity and Specificity, error rate, and false classification ratio. Finally, the efficiency of the healthy and faulty motor is compared through finite element analysis.

In this work, thermal images are captured at three load conditions such as no-load, half load, and full load. Thermal signatures are provided based on temperature range at no load, half load, and full load conditions that have been illustrated in figures 12, 13, and 14.

The accuracy, sensitivity, and specificity of proposed fault classifier and existing methods have been estimated using the following equations (10-12):

$$Sensitivity = \frac{TP}{TP + FN} \tag{10}$$

$$\text{Specificity} = \frac{TN}{TN + FP} \tag{11}$$

$$Accuracy = \frac{TP + TN}{TP + FN + TN + FP} \tag{12}$$

Where TP indicates the True Positive, TN represents the True Negative; FP will be the False Positive, and FN represents the False Negative. A number of properly detected and classified motor fault pixels in the thermal image have been defined by the TP and the number of imperfectly detected and classified motor fault pixels has been explained by the TN. FP will determine the number of incorrectly detected and classified fault part pixels of the thermal image, and the number of incorrectly detected and classified non-fault part pixels in the thermal image is defined by FN.

Figure 15 shows the proposed and existing methods' performance analysis. From figure 15, the proposed fault classifier has taken 95.8% accuracy; 94% sensitivity, and 93.9%

specificity during the motor fault detection in the specificity of the thermal image than existing methods ANN, CNN, and SVM. Hence, the proposed fault classifier can provide effective performance.

The selection of thermography over vibration and current-based techniques for motor fault detection, Table 4 emphasizes thermography's unique advantages and its quantitative edge. Despite the higher initial cost of thermographic cameras, their extensive utility, coupled with lower maintenance needs, provides significant cost-effectiveness.

Thermography's broad fault detection capabilities, effectively identifying both mechanical and electrical issues, mark a substantial advantage. It excels in early overheating detection, a key indicator of potential failures, thus enhancing preventative maintenance strategies.

Thermography's ability to remotely detect faults is particularly beneficial for motors in hard-to-reach places, such as high altitudes or deep pits, ensuring safe and effective monitoring without direct access. The non-invasive nature of thermography provides a substantial advantage in these contexts. It enables remote inspection capabilities, eliminating the need for direct physical interaction with the equipment. Conversely, the application of vibration analysis in such settings is hindered by the logistical difficulties associated with the placement and maintenance of sensors in these hard-to-reach areas. While current analysis methods are somewhat more manageable, as they primarily require access to the electrical connections of the motor, issues related to the positioning and ongoing maintenance of these sensors still present notable challenges in such environments.

Figure 16 shows the various analysis comparisons for fault detection. Figure 16 has demonstrated that the thermography method has given high percentage of fault detection accuracy in condition monitoring compared to the vibration and current analysis.

The comparison chart of error rate in proposed and existing methods has been established in figure 17. The proposed automated motor fault detection and classification system have given the low percentage of error rate during the fault detection and classification in the motor’s target thermal image compared to existing methods.

The false fault classification ratio of presented and existing works is given in figure 18. From the comparison chart, it clearly says that the proposed integrated faster R-CNN-SURF classifier system can give a low percentage of false classification ratio in the process of motor fault classification compared to existing methods ANN, CNN, and SVM. Hence, an improved classifier can give effective fault classification in the target thermal image at an early stage.

Figure 19 shows the efficiency of the proposed efficiency and existing efficiency estimation method. In this study, efficiency has been estimated with the help of finite element analysis according to the speed and torque. In figure 19, the proposed method has given high efficiency compared to the existing theoretical efficiency estimation method.

4. Conclusion

In this paper, improved image processing and machine learning methods have been used to detect and classify induction motor faults at an early stage using thermal images. Thermography emerges as a formidable method for motor fault detection, offering comprehensive benefits in operational safety, efficiency, and fault detection range. This makes it an invaluable tool in predictive maintenance, particularly in challenging operational conditions, thereby standing as a strong alternative and complement to vibration and current-based techniques. It is worked on thermal images of induction motor at various loading conditions and faulty conditions. The image preprocessing has been done with second level 3D-DWT and the macro color texture features are extracted using Gabor filter, and micro color and texture features are extracted by GNS map. The faster R-CNN was integrated with the SURF method to improve the fault classification accuracy. In this enhanced classifier, the feature descriptor has been used with SURF for the feature selection and matching process and afterward, faster-RCNN is computed to fault classification by eliminating the mismatches according to the selected features. The induction motor faults such as bearing faults, stator faults, and rotor faults has been detected and classified at an early stage. Finally, the efficiency of the healthy and faulty motor is estimated with the help of finite element analysis. Hence, the energy will be preserved through early fault deletion using this proposed method during the operations.

References

1. Agoston, K., “Fault detection of the electrical motors based on vibration analysis”, Procedia Technology, vol.19, pp. 547-553, 2015.
2. De Araujo Cruz, A.G., Gomes, R.D. and Belo, F.A., et al., “A hybrid system based on fuzzy logic to failure diagnosis in induction motors”, IEEE Latin America Transactions, vol.15, no.8, pp.1480-1489, 2017.
3. Chang, H.C., Jheng, Y.M., Kuo, C.C., et al., “Induction motors condition monitoring system with fault diagnosis using a hybrid approach”, Energies, vol.12, no.8, pp.1-12, 2019.
4. Contreras-Hernandez, J.L., Almanza-Ojeda, D.L., Ledesma-Orozco, S., et al. “Quaternion signal analysis algorithm for induction motor fault detection”, IEEE Transactions on Industrial Electronics, vol.66, no.11, pp. 8843 – 8850, 2019.
5. Chen, Y.T., Lai, J.C., Jheng, Y.M., et al., “Partial discharge detection for stator winding insulation of motors using artificial neural network”, Advances in Mechanical Engineering, vol.10, no.7, pp.1-10, 2018.
6. Delgado-Prieto, M., Carino-Corrales, J.A., Saucedo-Dorantes, J.J., et al., “Thermography Based Methodology for Multifault Diagnosis on Kinematic Chain”, IEEE Transactions on Industrial Informatics, vol.14, no.12, pp. 5553 – 5562, 2018.
7. Javed, M.R., Shabbir, Z., Asghar, F., et al., “An efficient fault detection method for induction motors using thermal imaging and machine vision”, Sustainability, vol. 14, no.15, 9060-9072, 2022.
8. Mahami, A., Rahmoune, C., Benazzouz, D., et al., “Induction motor condition monitoring using infrared thermography imaging and ensemble learning techniques”, Advances in Mechanical Engineering, pp. 1-7, 2021.
9. Talhaoui, H., Ameid, T., Aissa, O., et al. “Wavelet packet and fuzzy logic theory for automatic fault detection in induction motor”, Soft Computing, vol. 26, pp. 11935–11949, 2022.
10. Lee, C.Y. and Cheng, Y.H., “Motor fault detection using wavelet transform and improved PSO-BP neural network”, Processes, vol. 10, pp. 1322-1341, 2020.

11. Singh, M. and Shaik, A.G., "Broken Rotor Bar Fault Diagnosis of a Three-phase Induction Motor using Discrete Wavelet Transform", IEEE PES GTD Grand International Conference and Exposition Asia (GTD Asia), pp.13-17, 2019.
12. Ge, M., Wang, J., Xu, Y., et al., "Rolling bearing fault diagnosis based on EWT Sub-modal hypothesis test and ambiguity correlation classification", Symmetry, vol.10, no.2, pp.1-15, 2018.
13. Lee, C.Y., Wen, M.S., Zhuo, G.L., et al., "Application of ANN in Induction-Motor Fault-Detection System Established with MRA and CFFS" Mathematics, vol. 10, no. 13, 2250, 2022.
14. Abdelmaksoud, M., Torki, M., El-Habrouk, M., et al., "Convolutional-neural-network-based multi-signals fault diagnosis of induction motor using single and multi-channels datasets", Alexandria Engineering Journal, vol. 73, pp. 231-248, 2023.
15. Chouhan, A., Gangsar, P., Mechefske, C.K., et al., "Artificial neural network–based fault diagnosis for induction motors under similar, interpolated and extrapolated operating conditions", Sage journals, vol. 52, no. 10, pp. 1-11, 2021.
16. Agrawal, P. and Jayaswal, P., "Diagnosis and classifications of bearing faults using artificial neural network and support vector machine", Journal of The Institution of Engineers (India): Series C, vol.101, pp. 61-72, 2020.
17. Jayaswal, P. and Wadhwani, A.K., "Application of artificial neural networks, fuzzy logic and wavelet transform in fault diagnosis via vibration signal analysis: A review", Australian journal of mechanical engineering, vol.7, no.2, pp. 157-171., 2015.
18. Ali, M.Z., Shabbir, M.N.S.K., Liang, X., et al., "Machine learning-based fault diagnosis for single-and multi-faults in induction motors using measured stator currents and vibration signals", IEEE Transactions on Industry Applications, vol.55, no.3, pp.1-14, 2019.
19. Xu, G., Liu, M., Jiang, Z, et al., "Bearing fault diagnosis method based on deep convolutional neural network and random forest ensemble learning", Sensors, vol.19, no.5, pp.1-21, 2019.
20. Lu, C., Wang, Y., Ragulskis, M., et al., "Fault diagnosis for rotating machinery: A method based on image processing", PLoS ONE 2016, 11, e0164111, 2016.

21. Mao, W., Ding, L., Tian, S., et al., “Online detection for bearing incipient fault based on deep transfer learning”, Measurement, vol.152, pp.1-23, 2020.
22. Zhao, R., Yan, R., Chen, Z., et al., “Deep learning and its applications to machine health monitoring”, Mechanical Systems and Signal Processing, vol.15, pp.213-137, 2019.
23. Gangsar, P. and Tiwari, R., “Signal based condition monitoring techniques for fault detection and diagnosis of induction motors: A state-of-the-art review”, Mechanical Systems and Signal Processing, vol.144, 106908, 2020.
24. Glowacz, A., “Fault diagnosis of single-phase induction motor based on acoustic signals”, Mechanical Systems and Signal Processing, vol.117, pp. 65-80, 2019.
25. Rahmat, T., Ismail, A., and Aliman, S., “Chest X-ray image classification using faster R-CNN”, Malaysian Journal of Computing, vol.4, no.1, pp. 225-236, 2019.
26. Khamisan, N., Ghazali, K.H. and Zin, A.H.M., “A thermograph image extraction based on color features for induction motor bearing fault diagnosis monitoring”, ARPN Journal of Engineering and Applied Sciences, vol.10, no.22, pp.17095-17101, 2015.
27. Kim, M.C., Lee, J.H., Wang, D.H., et al., “Induction motor fault diagnosis using support vector machine, neural networks, and boosting methods”, Sensors, vol. 23, no. 5, 2585, 2023.

LIST OF FIGURES

LIST OF TABLES

APPENDICES

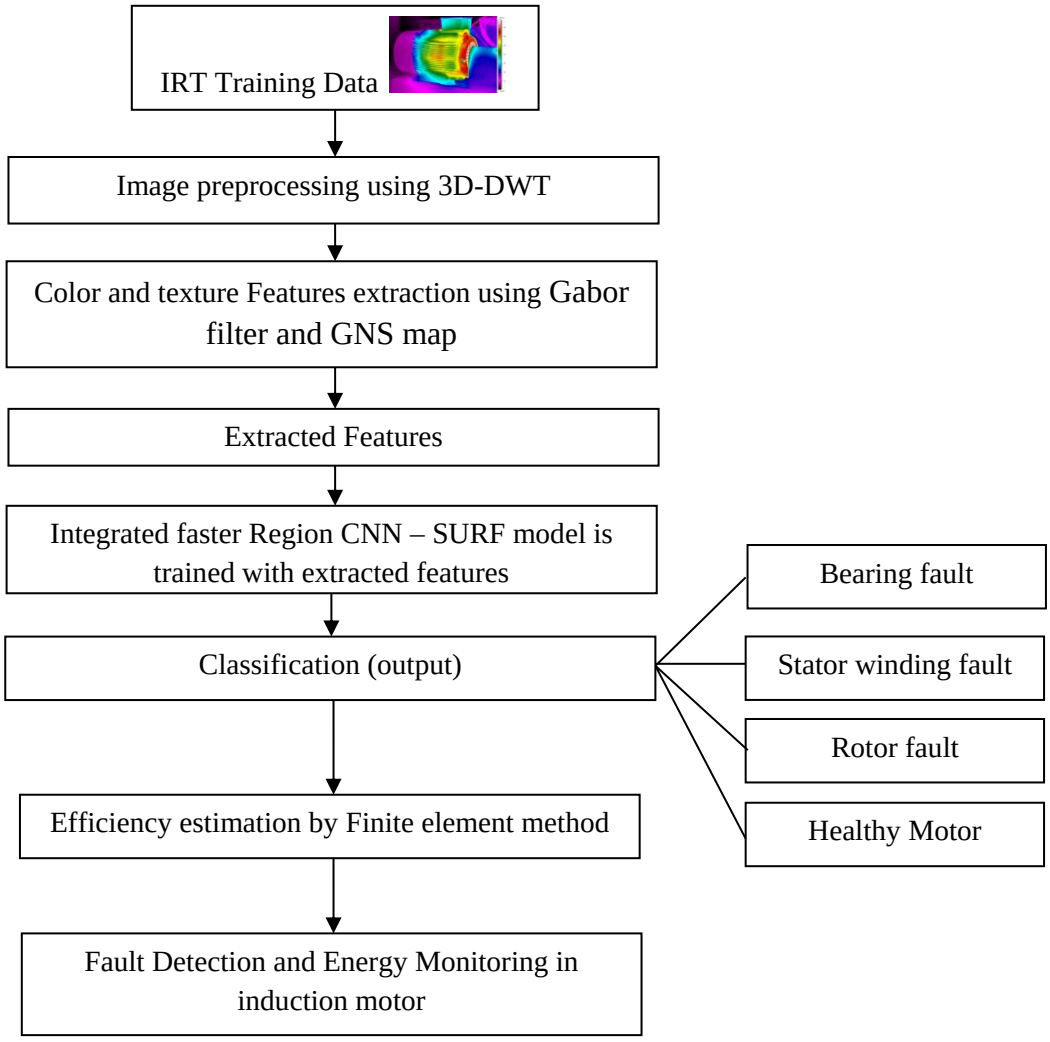

Figure 1 Proposed System Architecture

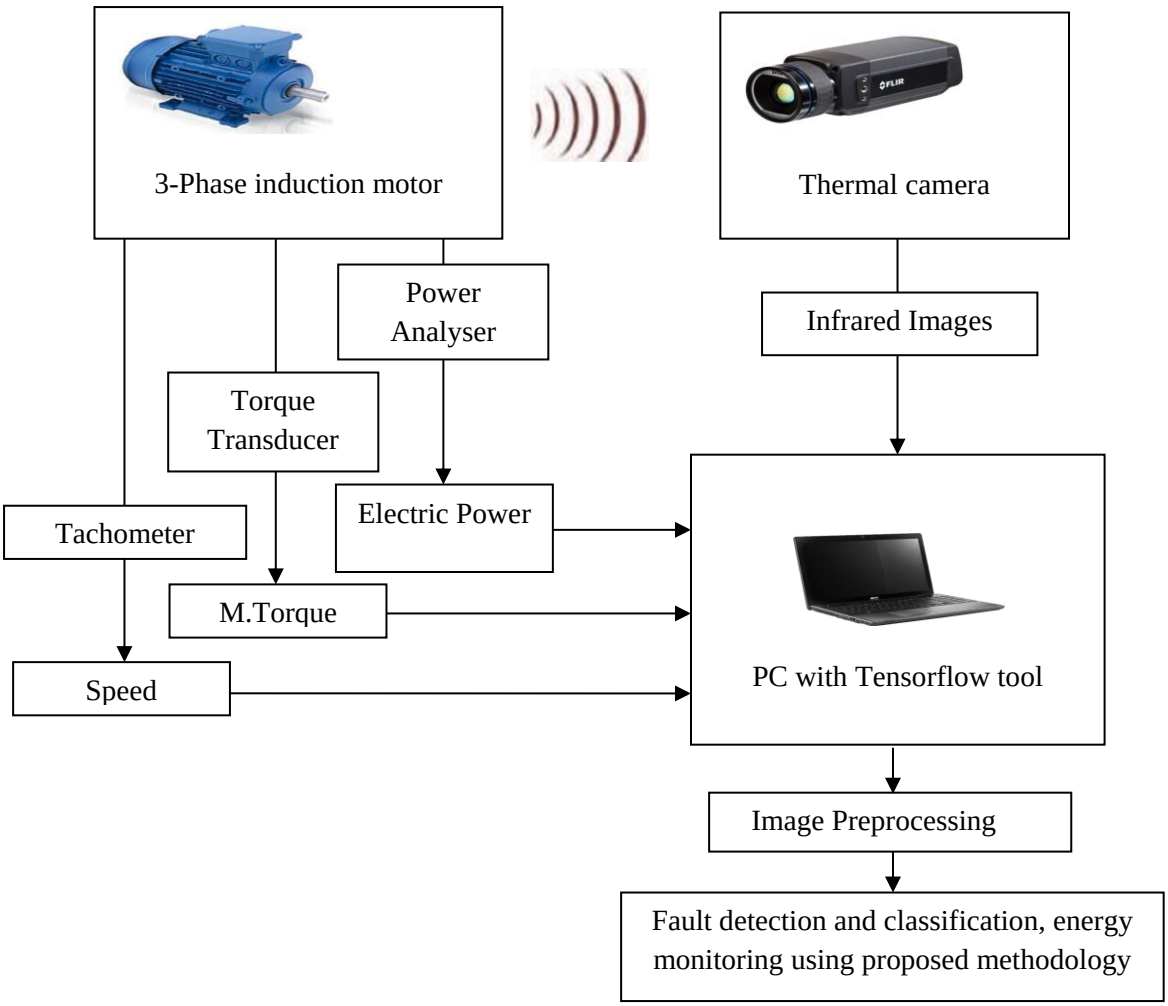

Figure 2 Experimental Test Bench

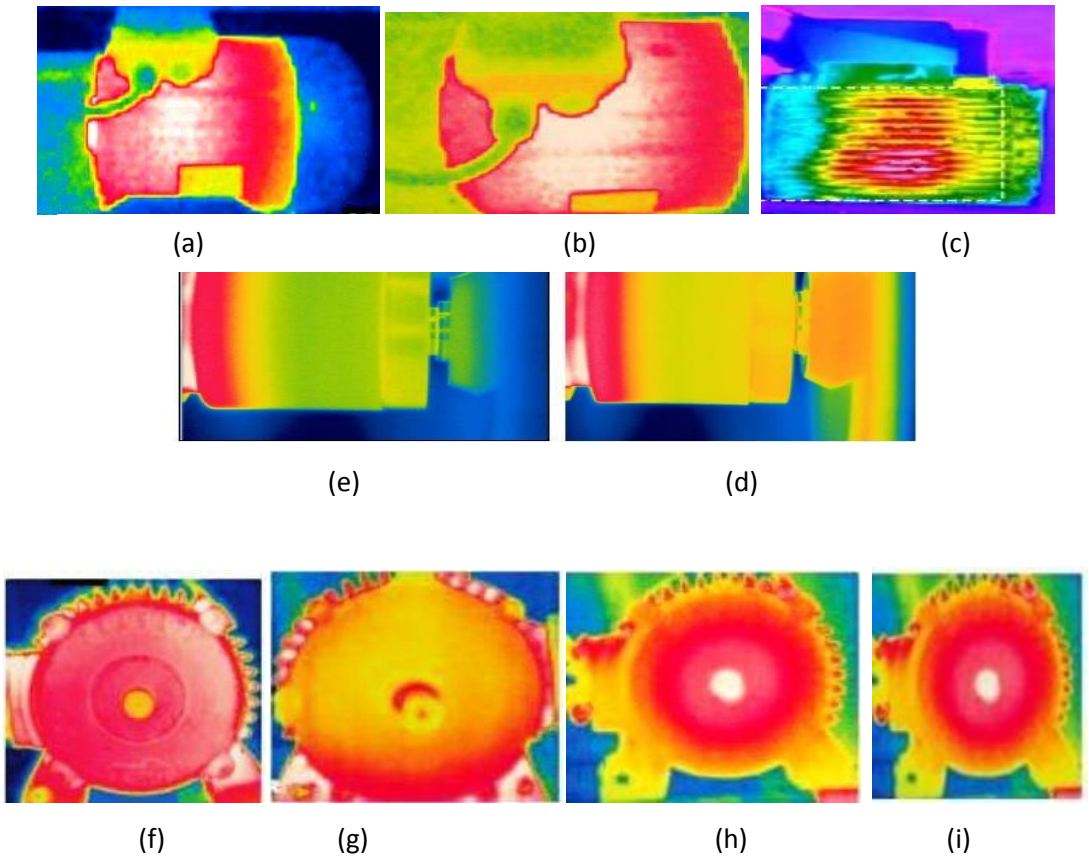

Figure 3 Sample thermal images (a) Healthy motor, (b) Rotor Bar Fault (c) Abnormal Stator (d) Normal Bearing (e) Abnormal Bearing (f) Inner race defect (Bearing) (g) Outer race defect (Bearing) (h) Healthy Bearing (i) Lubrication Lack (Bearing)

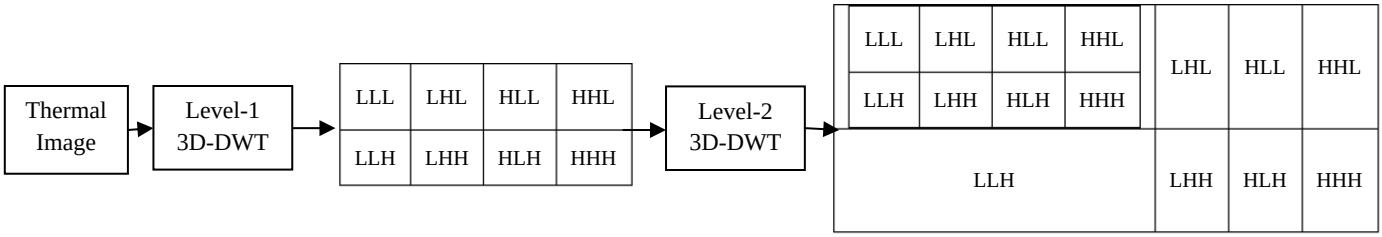

.Figure 4 Two-level 3D-DWT

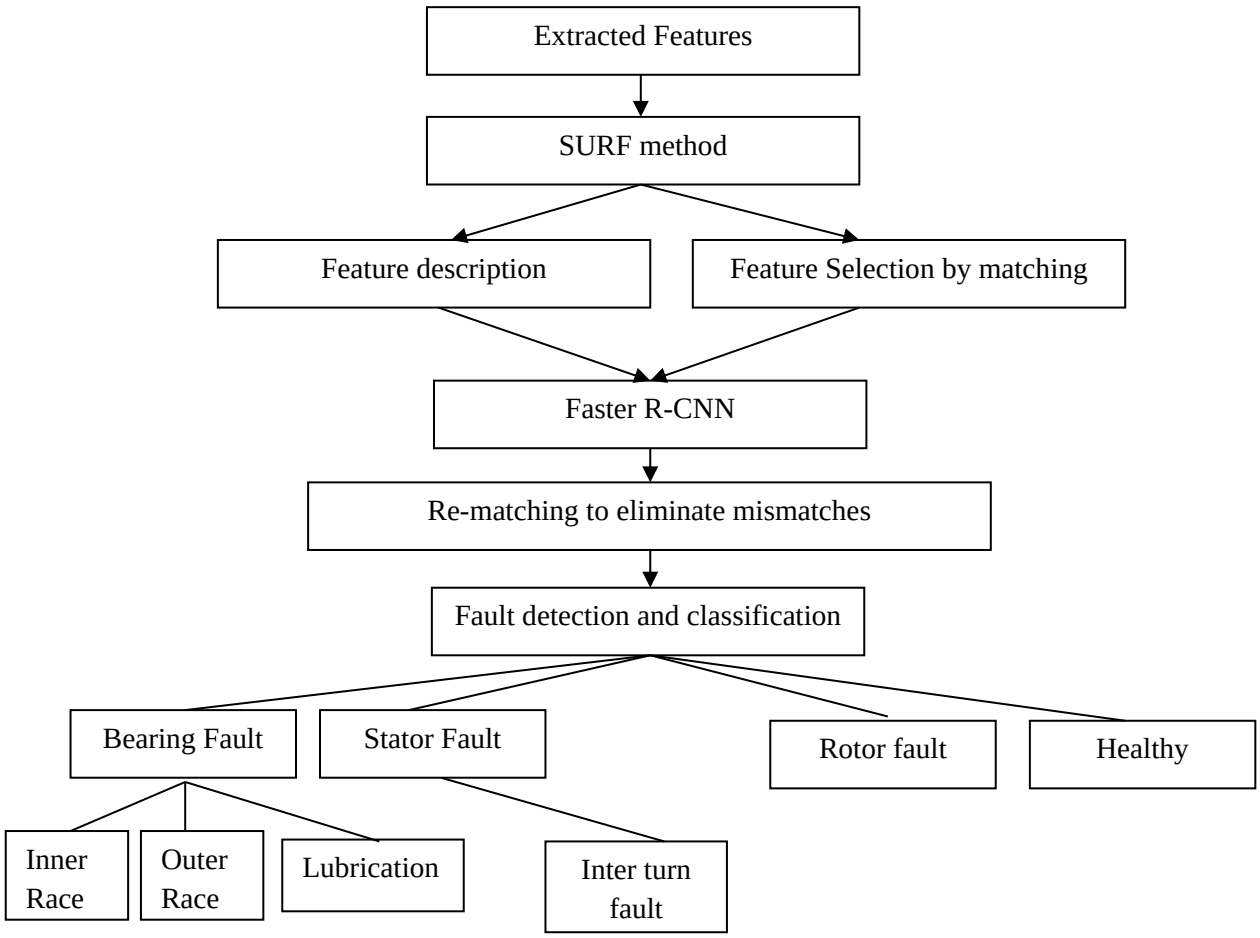

Figure 5 Integrated faster RCNN-SURF

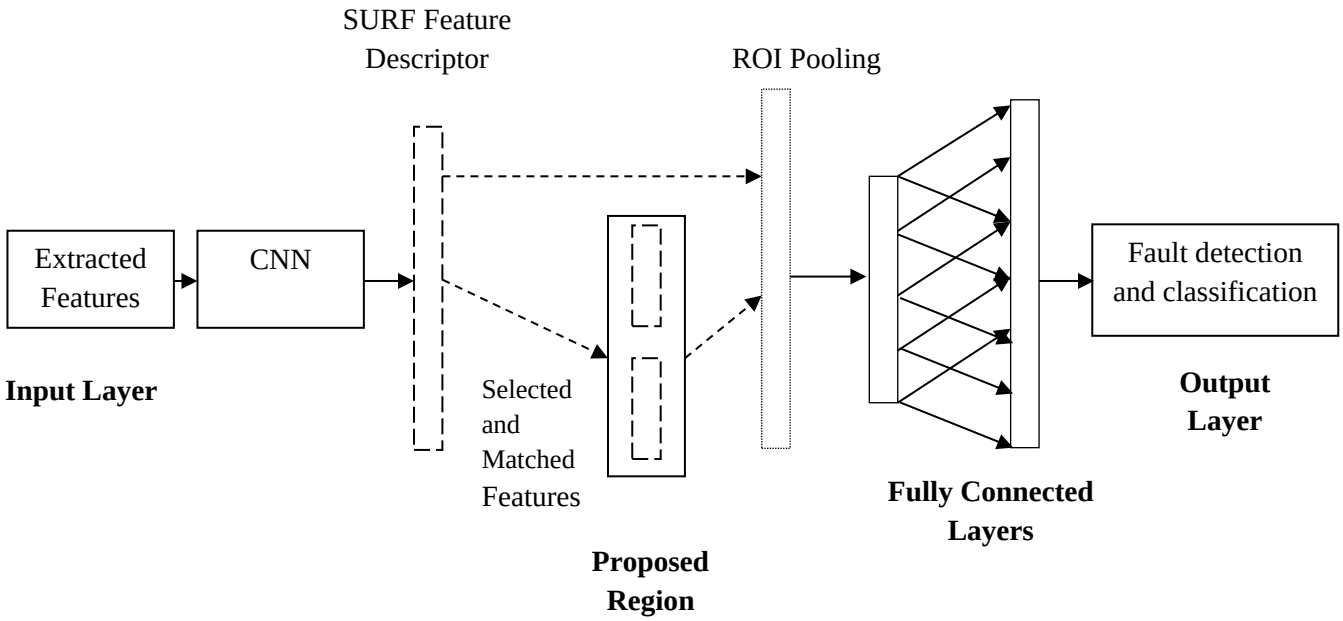

Figure 6 Proposed faster RCNN-SURF Architecture

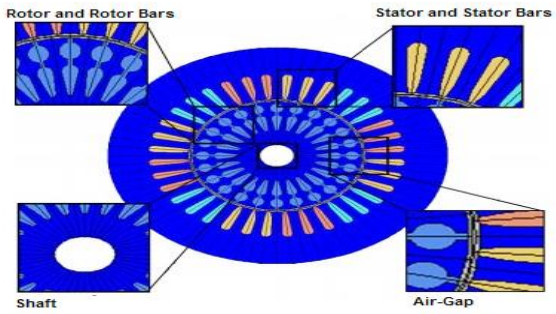

Figure 7 Induction Motor flux distribution in 2D view for 0.55A stator current and 1280rpm speed

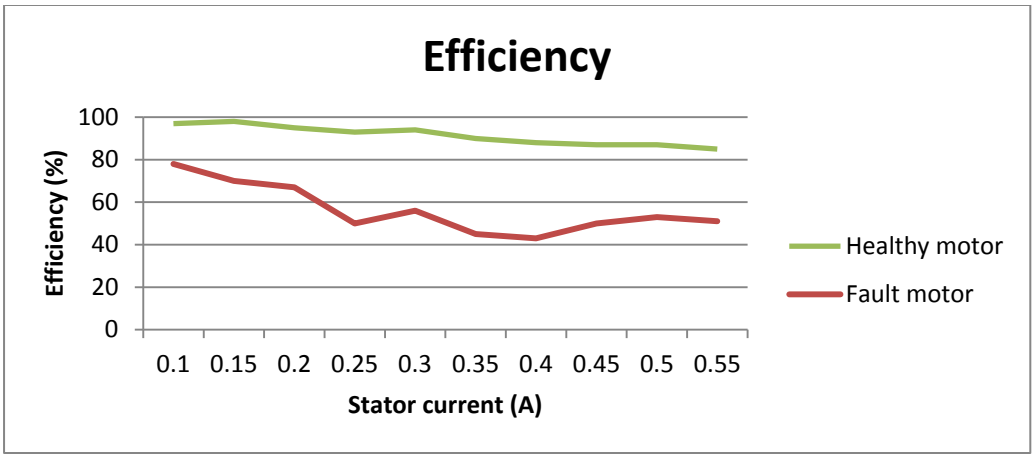

Figure 8 Efficiency between healthy and fault induction motor

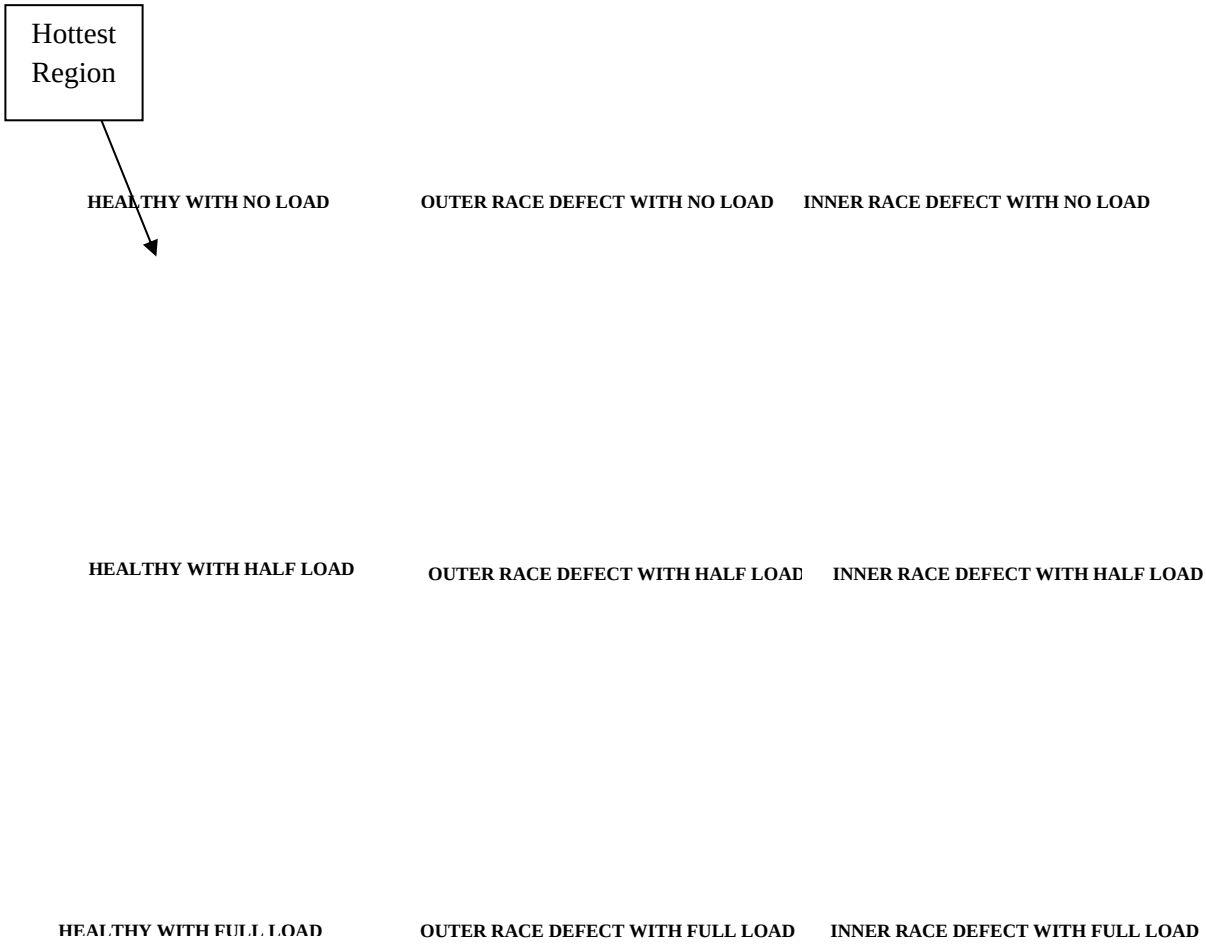

Figure 9 Sample images with no load, half load, and full load for healthy and bearing faults

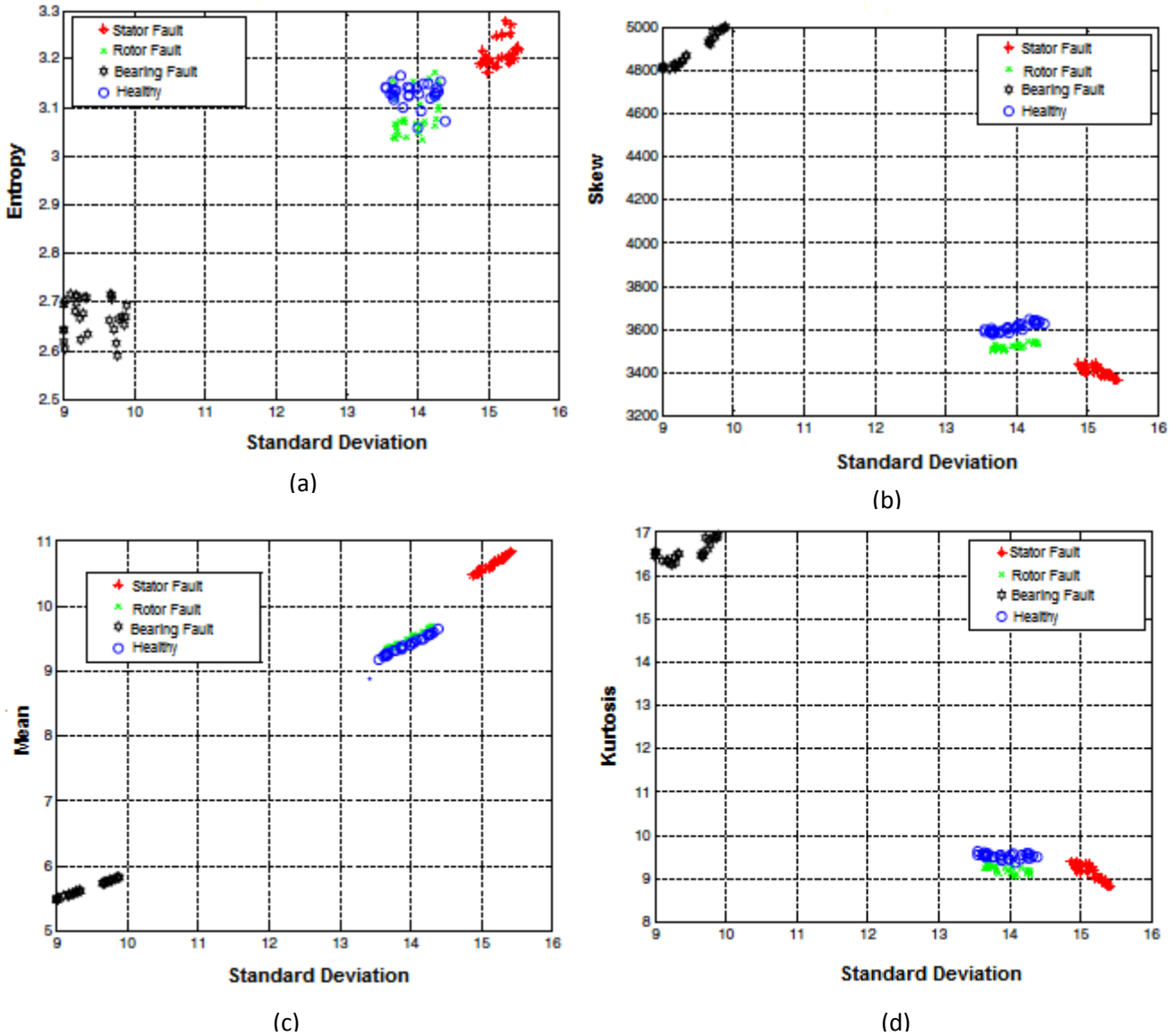

Figure 10 Features presentation in RGB color space for the fault classification: (a) Entropy versus standard deviation, (b) Skew versus standard deviation, (c) Mean versus standard deviation, (d) Kurtosis versus standard deviation

Predicted label							
0	360 16.6%	0 0.0%	0 0.0%	0 0.0%	0 0.0%	0 0.0%	100% 0.0%
1	0 0.0%	334 16.7%	5 0.0%	5 0.0%	10 0.0%	6 0.0%	92.28% 7.72%
2	0 0.0%	0 0.0%	359 16.7%	0 0.0%	0 0.0%	1 0.0%	99.72% 0.28%
3	0 0.0%	0 0.0%	0 0.0%	358 16.6%	0 0.0%	2 0.0%	99.44% 0.0%
4	0 0.0%	3 0.0%	1 0.0%	0 0.0%	366 16.7%	0 0.0%	98.89% 1.11%
5	0 0.0%	4 0.0%	3 0.0%	0 0.0%	0 0.0%	353 16.7%	98.06% 1.94%
	100% 0.0%	97.94% 2.06%	97.55% 2.45%	98.62% 1.38%	97.35% 2.47%	97.51% 2.49%	98.19% 1.81%
	0	1	2	3	4	5	

Actual label

Figure 11 Confusion matrix for fault detection

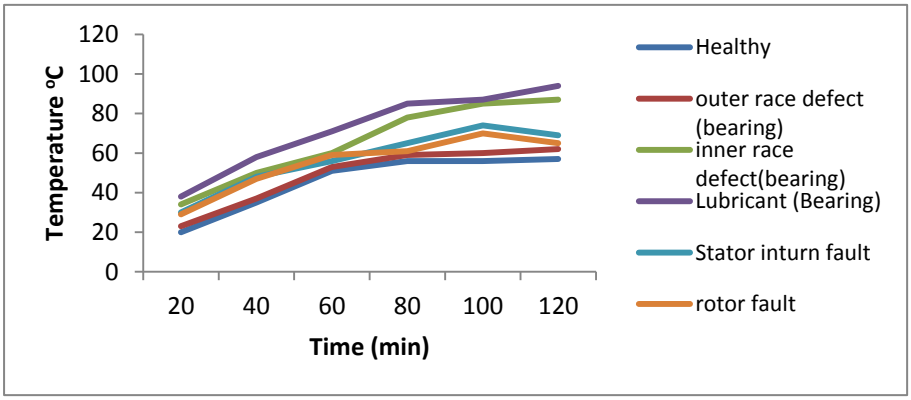

Figure 12 Thermal signatures at no load condition

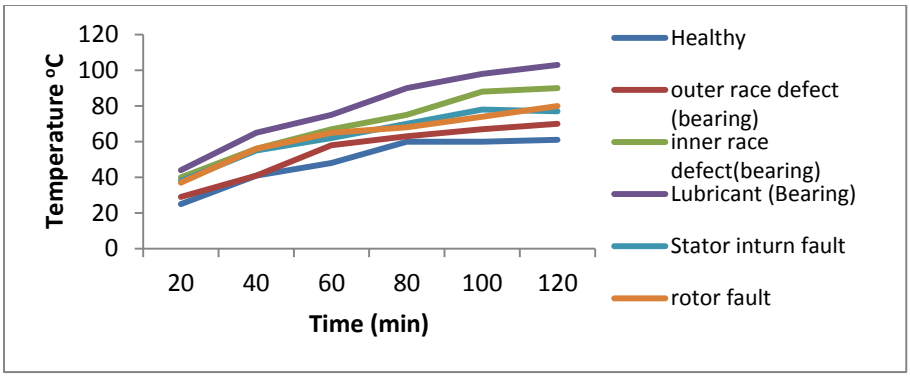

Figure 13 Thermal signatures at half load condition

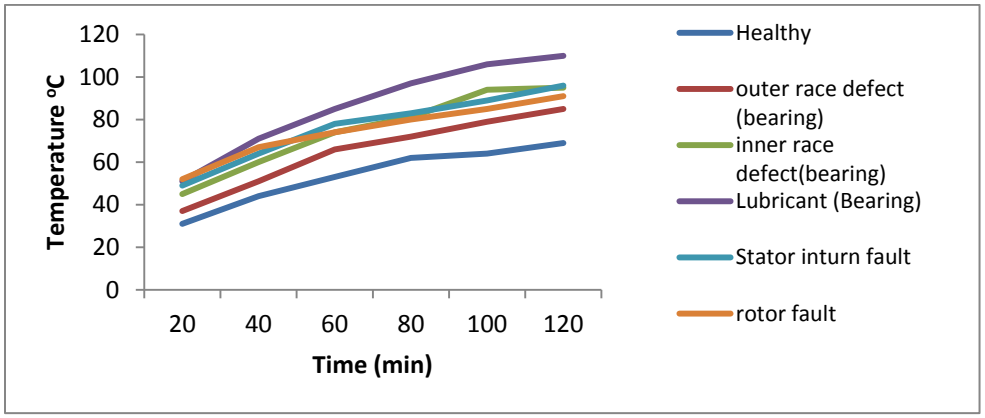

Figure 14 Thermal signatures at full load condition .

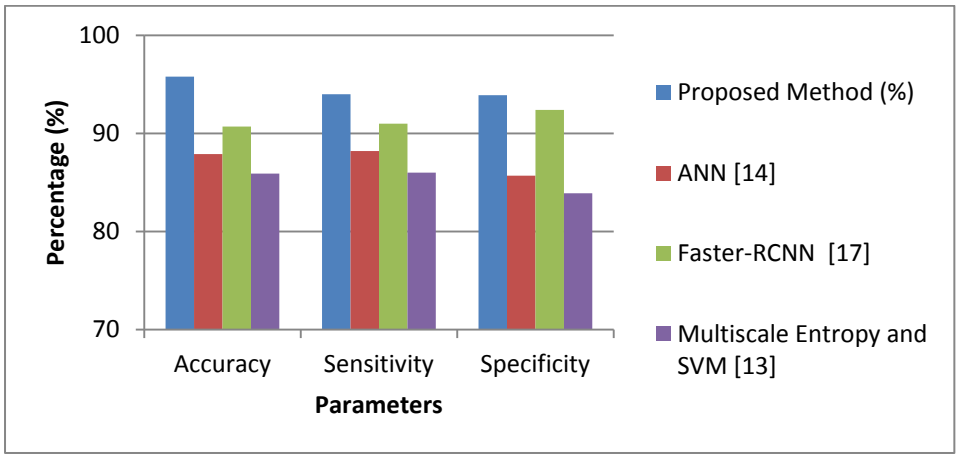

Figure 15 Performance analysis of proposed method

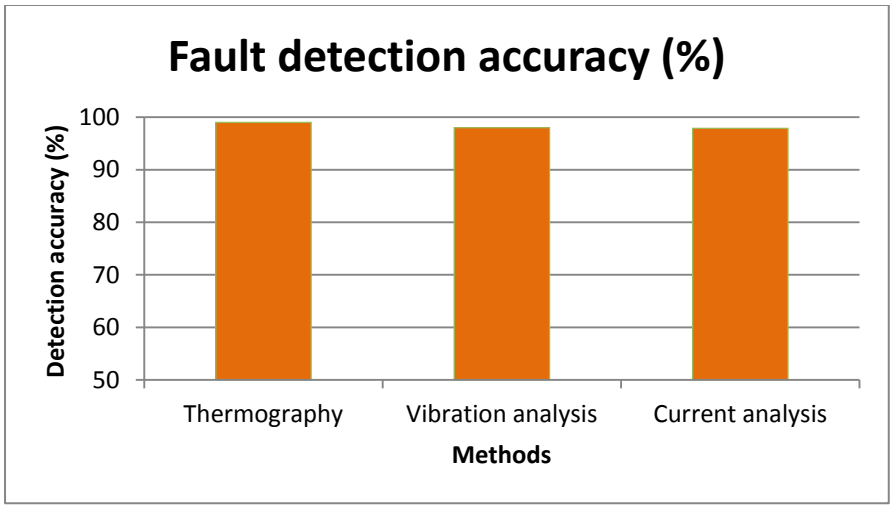

Figure 16 Comparison chart of various analysis for fault detection

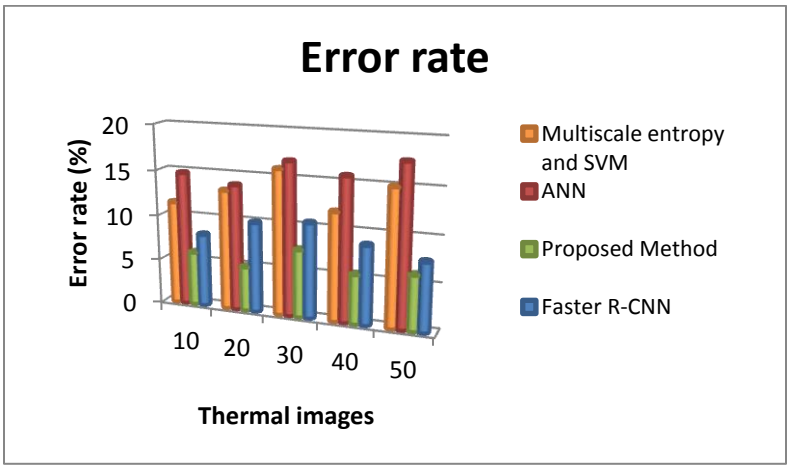

Figure 17 Error rate

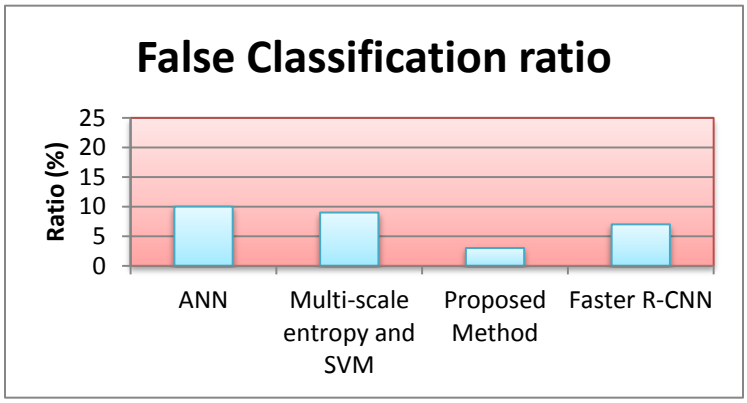

Figure 18 False classification ratio

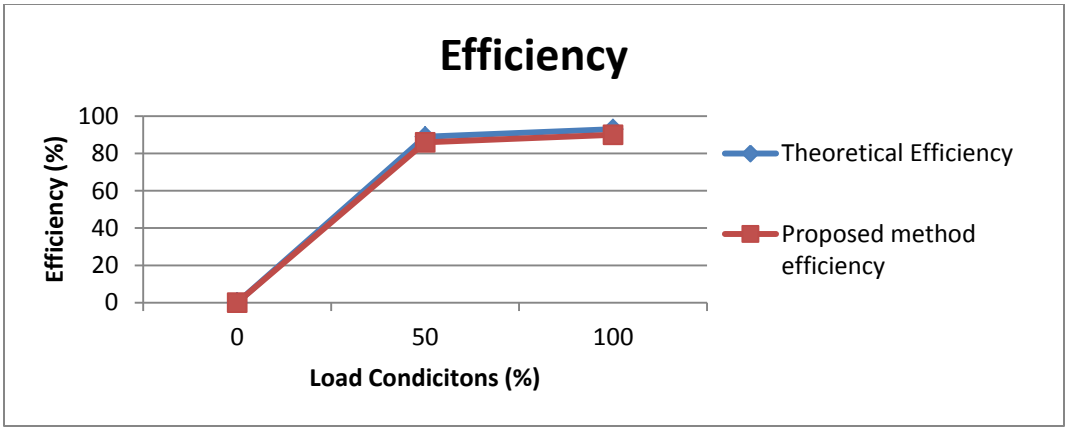

Figure 19 Efficiency of proposed and existing methods

Table 1 Technical Specifications

Parameters	Specifications
Processor	Intel core I3
Hard Disk	500 GB
Monitor	15 VGA Color.
Mouse	Logitech
RAM	2GB
Operating System	Windows 7, 64 bit
Program Software Program Language	TensorFlow Tool Python 3.5

Table 2 Specifications of induction motor and thermal camera

S.No.	Device Name	Specifications
1.	Induction motor	Power Supply : 3 phase, 440V, 50Hz, 0.55A Power : 0.5 HP Speed: 1280rpm
2.	Thermal Camera	Storage Temperature range: -20°C to +2000°C Spectral Range : 7.5 to 13 μ m Thermal Sensitivity: <0.05^{o}C@30^{o}C Pixels: 640 × 480 Focal Length: 13.1mm

Table 3 Image data details

Machine conditions	Data file	Image data dimension	Total data file	No.of features	Features dimension at each level
Healthy	33	640×480	132	Five features (Skew, entropy, mean, standard deviation, and kurtosis)	120 × 6
Stator Fault	33				
Rotor Fault	33				
Bearing Fault	33				

Table 4 Comparison between motor fault detection methods

Parameter	Thermography-Based	Vibration-Based	Current-Based
Detection Method	Non-contact	Contact (requires accelerometers)	Contact (requires MCSA sensors)
Fault Types Detected	Both electrical and mechanical faults	Primarily mechanical faults	Primarily electrical faults
Early Detection of Overheating	Very effective in early detection of overheating	Less effective in early detection of overheating	Less effective in early detection of overheating
Preventive Maintenance	Very effective	Effective for certain issues	Effective for certain issues
Inspection Coverage	Large coverage	Limited to specific areas where sensors are installed	Focused on electrical characteristics; limited mechanical insight
Interference and Environmental Independence	Free from electromagnetic interference and environment independent	Sensitive to external noise and vibrations	Performance can be affected by load changes
Applicability in High-Voltage Settings	Yes	May require additional measures	Yes (depending on the sensors)
Reliability	High (consistent in diverse conditions)	High (accurate for mechanical issues)	Moderate (can vary with load conditions)
Cost (Long-Term)	Cost-effective (broad detection, less maintenance)	Higher (due to maintenance and installation)	Moderate
Safety and Operational Impact	High (non-intrusive, no direct access needed)	Moderate (noise, installation challenges)	High
Performance in High Heights/Deep Pits	Very effective (remote operation advantageous)	Challenging (access and sensor placement issues)	Effective (limited by sensor placement, but feasible)
Equipment Requirement	Standard thermographic equipment	Requires specialized vibration analysis equipment	Requires specialized MCSA sensors

Author's Brief Biographies:

Author:1

SASIKUMAR B is an Associate Professor in the department of Artificial Intelligence and Data Science at Knowledge Institute of Technology, Salem, and Tamilnadu, India. He received his bachelor's degree B.E. in Electrical and Electronics Engineering from Sengunthar Engineering College and Master's degree in Computer Science and Engineering from Anna University Trichirappalli. He is a life member of the Indian Society for Technical Education. His work focuses on Image mining, Machine learning, Artificial Intelligence and Energy Conservation.

Author:2

Dr.K.Venkatasalam was born on January 24, 1981 in Salem. He obtained his Diploma in Computer Technology at Rajaji Institute of Technology and obtained his U.G Degree in Computer Science and Engineering at Mahendra Engineering College Affiliated to Periyar University , Salem , in 2003 and Master of Engineering (M.E) Degree in Computer Science and Engineering at Arunai Engineering College Affiliated to Anna University , Chennai, in 2005 .He has done his research in the area of image Mining and obtained doctorate from Anna University in 2017.He has Started his teaching profession in the year of 2006.At present he is an Associate Professor in the Department of Computer Science and engineering in Mahendra Engineering College, Namakkal. He has published 18 research papers in International and National Journals as well as conferences. He is a life member of the Indian Society for Technical Education member of the Institutions of Engineers IE(I) and Computer Society of India (CSI). His technical interests include Image mining, Big Data, Cloud Computing, Artificial Intelligent and Internet of Things. Currently, eight scholars are pursuing their Ph.D. under his supervision.

Author:3

Dr. RAJENDRAN P was born on July 2, 1974 in Namakkal. He obtained his Master of Engineering (M.E) Degree in Computer science and engineering from Anna University, Chennai, in 2005. He has started his teaching profession in the year 2000 in K.S.Rangasamy College of Technology and worked from 2000 to 2010. At present, he is a Professor in the department of computer science and engineering and Director - Placement at Knowledge Institute of Technology, Salem. He has guided more than 30 U.G and P.G projects. He has published 30 papers in various National and International Journals and Conferences related to his research work. He has also published a part of his research work in Springer and Journal of Medical Systems. He is a life member of the Indian Society for Technical Education. He is also a member of International Association of Engineers (IAENG). His technical interests include Data Mining, Image Mining, Bio-Medical Engineering, Soft Computing, Computer Networks and Neural Networks. Guided by his mentorship, seven scholars have successfully completed their Ph.D., and he is currently supervising eight scholars.